ELSEVIER

Journal of Alloys and Compounds 434–435 (2007) 176–179

Journal of ALLOYS AND COMPOUNDS

www.elsevier.com/locate/jallcom

Fe-based bulk metallic glasses with Y addition

Tanya Aycan Baser, Marcello Baricco *

Dipartimento di Chimica IFM and NIS, Università di Torino, Via P.Giuria, 9-10125 Torino, Italy

Available online 13 October 2006

Abstract

This paper aims to study the role of residual vacuum during sample preparation and of quenching rate on glass formation in $Fe_{50-x}Cr_{15}Mo_{14}Y_xC_{15}B_6$ ($x=0$, 2) alloys. The equilibrium phase mixture has been clarified for both alloys, combining X-ray diffraction (XRD) and scanning electron microscopy (SEM) measurements. The beneficial effects of minor addition of Y on the glass formation are evidenced. A high residual vacuum during sample preparation promotes glass formation. Glass transition temperature for amorphous sample containing 2 at.% Y is 881 K and the onset crystallization temperature is 904 K. The melting behavior for both as-cast alloys were measured with high temperature differential scanning calorimeter (HTDSC). Melting starts at 1384 K, ends at 1506 and 1470 K as liquidus temperatures for $Fe_{50}Cr_{15}Mo_{14}C_{15}B_6$ and $Fe_{48}Cr_{15}Mo_{14}Y_2C_{15}B_6$ alloys, respectively. The addition of Y leads to a melting behavior of as-cast sample close to eutectic, which enhances glass formation.
© 2006 Elsevier B.V. All rights reserved.

Keywords: Amorphous materials; X-ray diffraction; Thermal analysis

1. Introduction

It is known that bulk metallic glasses (BMGs) combine high strength with high corrosion resistance properties, which cannot be achieved by from crystalline alloys. The glass forming ability (GFA) of Fe-based alloys is improved by an addition of suitable quantities of metalloids, early transition metals and simple metals [1]. It was also found that appropriate minor alloying additions were very effective in increasing GFA, enhancing thermal stability and improving mechanical properties of BMGs [2]. In particular, additions of large atoms, such as Y, is very helpful in terms of glass formation [3]. The glass formability of Fe-based alloys was found to improve significantly as more Er/Y was added to the base alloy [4]. It has been suggested that elemental Y played the role as oxygen scavenger in these Fe–Cr–Mo–C–B alloys, leading to the suppression of heterogeneous nucleation of crystal phases and to improved glass formability [5]. On the other hand, the glass formation in Fe-based alloys with Y addition was claimed to be favored thermodynamically [6]. In fact, melting behavior of selected alloys showed that the addition of Y effectively shifts the alloy composition from off-eutectic close a eutectic point.

In this paper, we investigated the role of yttrium on glass formation in $Fe_{50-x}Cr_{15}Mo_{14}Y_xC_{15}B_6$ ($x=0$, 2) alloys. The study is focused on the effect of sample preparation conditions to understand the role of oxygen on GFA. Casting of liquid alloys in a conic shaped mould allows also the study of the effect of quenching rate on glass formation. So, both the role of residual vacuum in the sample preparation chamber and the ingot diameter on sample microstructures was investigated. In order to understand the effect of Y addition on melting behavior, as-cast alloys were investigated by thermal analysis (HTDSC).

2. Experimental

Master alloys ($Fe_{50}Cr_{15}Mo_{14}C_{15}B_6$ and $Fe_{48}Cr_{15}Mo_{14}Y_2C_{15}B_6$) have been prepared from pure elements by arc melting in a furnace under Ar atmosphere. Each ingot was melted several times in order to obtain a good homogeneity. In order to study the effect of oxygen on GFA, the liquid alloys were cast in a conic shaped copper mould using different residual vacuum in the sample preparation chamber. X-ray diffraction (XRD) was performed to examine the structure of the samples using Co Kα radiation on a Philips PW1830 diffractometer. Microstructure analyses have been carried out by Leika Stereoscan 420 scanning electron microscopy (SEM). Thermal analysis was performed using Setaram high temperature differential scanning calorimeter (HTDSC) and Perkin-Elmer DSC7 at a heating rate of 0.17 K/s. The sample was contained in an alumina pan with some alumina powder to prevent sticking to the crucible walls. For high temperature measurements, the calorimetric cell was evacuated and purged several times before measuring under flowing He. Calibration of the instrument has been performed from the temperature and heat of fusion of pure metals (Al, Ag, Au, Fe, Cu, Ni).

* Corresponding author. Tel.: +39 011 670 7569; fax: +39 011 670 7855.
E-mail address: marcello.baricco@unito.it (M. Baricco).

0925-8388/$ – see front matter © 2006 Elsevier B.V. All rights reserved.
doi:10.1016/j.jallcom.2006.08.190

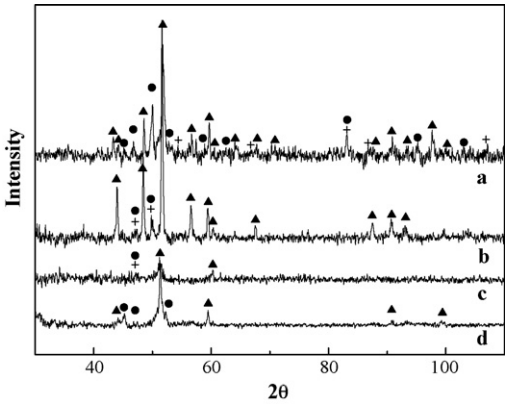

Fig. 1. XRD patterns of $Fe_{50}Cr_{15}Mo_{14}C_{15}B_6$ alloy: master alloy (a), as-cast top part (b), middle part (c) and bottom part (d). Symbols correspond to $M_{23}C_6$ (▲) M_6C (+) and M_7C_3 (●) phases. Casting was performed with a residual vacuum of 10^3 Pa.

3. Results and discussion

The effect of quenching rate on bulk glass formation in $Fe_{50}Cr_{15}Mo_{14}C_{15}B_6$ alloy is shown in Fig. 1, where XRD pattern of master alloy is compared to those taken from various slices of as-cast sample. Casting was carried out in presence of oxygen, with a residual vacuum in the sample preperation chamber of 10^3 Pa. The XRD patterns of master alloy can be fully indexed considering $M_{23}C_6$, M_6C, M_7C_3 crystalline phases. $M_{23}C_6$ and M_7C_3 phases were also observed in all slices of as-cast sample, whereas M_6C phase was observed only on the top of the ingot, because of the reduced quenching rate. All samples show sharp crystalline peaks, suggesting fully crystallized structures.

The microstructure of $Fe_{50}Cr_{15}Mo_{14}C_{15}B_6$ master alloy was observed by SEM (backscattered image), as shown in Fig. 2(a). EDS analysis was performed only for metals, because B and C cannot detected with occuracy. Considering B behaving like C in the carbide phases, the average atomic weight was estimated for $M_{23}C_6$, M_6C and M_7C_3 crystalline phases in order to obtain an interpretation of SEM pictures. EDS analysis showed that phase I is enriched in Mo (53 at.%), whereas an enrichment in Cr was observed in phase II (37 at.%) and in phase III (33 at.%). According to the EDS results and to the estimated average atomic weight, these phases have been assigned to Fe_3Mo_3C, $Cr_{23}C_6$ and Cr_7C_3 crystal structure, respectively, in

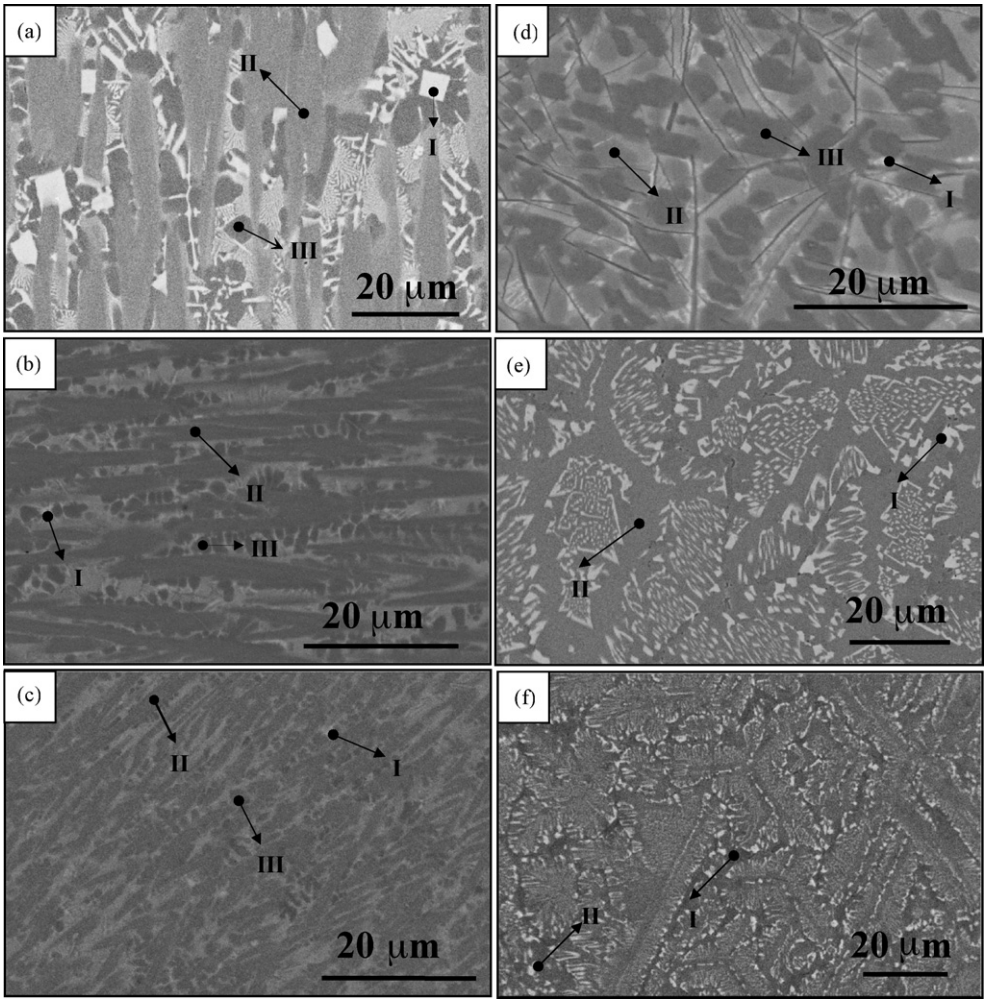

Fig. 2. SEM backscattered electron images for: $Fe_{50}Cr_{15}Mo_{14}C_{15}B_6$ master alloy (a), as-cast sample top part (b) and middle part (c); $Fe_{48}Cr_{15}Mo_{14}Y_2C_{15}B_6$ master alloy (d), as-cast sample top part (e) and middle part (f). Casting was performed with a residual vacuum of 10^3 Pa. The zones I, II and III were analysed by EDS.

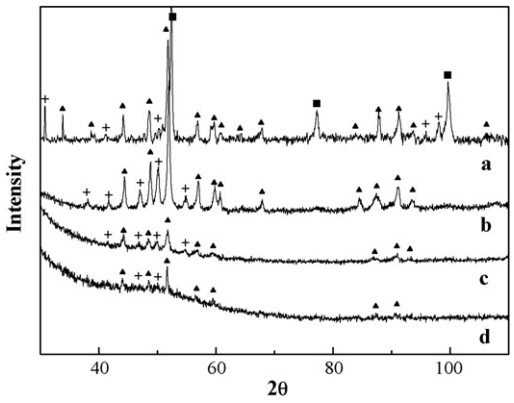

Fig. 3. XRD patterns of $Fe_{48}Cr_{15}Mo_{14}Y_2C_{15}B_6$ alloy: master alloy (a), as-cast top part (b), middle part (c) and bottom part (d). Symbols correspond to bcc-Fe (■), $M_{23}C_6$ (▲) and M_6C (+) phases. Casting was performed with a residual vacuum of 10^3 Pa.

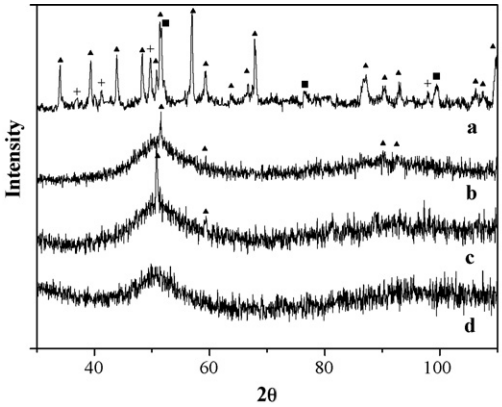

Fig. 4. XRD patterns of $Fe_{48}Cr_{15}Mo_{14}Y_2C_{15}B_6$ alloy: master alloy (a), as-cast top part (b), middle part (c) and bottom part (d). Symbols correspond to bcc-Fe (■), $M_{23}C_6$ (▲) and M_6C (+) phases. Casting was performed with a residual vacuum of 10^0 Pa.

agreement with XRD results shown in Fig. 1. The microstructures of $Fe_{50}Cr_{15}Mo_{14}C_{15}B_6$ as-cast samples taken from the top and the middle parts of the ingot are shown in Fig. 2(b and c), respectively. It is seen that the grain size decreased and the microstructure is refined, as the ingot diameter decreased, because of the increased quenching rate. From the EDS analysis of the microstructure shown in Fig. 2(b), an enrichment in Mo (29 at.%) was observed in phase I and enrichment in Cr was observed in phase II (41 at.%) and phase III (19 at.%), confirming the carbide phases identification. Reducing the ingot diameter M_6C phase became infrequent and decreased in size, but $M_{23}C_6$ and M_7C_3 phases continued to appear. Crystalline phases could not be observed by SEM on the bottom part of the as-cast sample, possibly because the phase compositions are close to each other, so that the relative contrast could not be achieved. It could also be related to the small size of crystals.

The effect of quenching rate on bulk glass formation in $Fe_{48}Cr_{15}Mo_{14}Y_2C_{15}B_6$ alloy is shown in Fig. 3. Casting was again carried out in presence of oxygen, with a residual vacuum in the sample preparation chamber of 10^3 Pa. The crystalline phases which were observed in the master alloys are $M_{23}C_6$, M_6C and bcc-solid solution. The microstructure of the $Fe_{48}Cr_{15}Mo_{14}Y_2C_{15}B_6$ master alloy was observed by SEM (backscattered image), as shown in Fig. 2(d). EDS analysis showed that only phase I contains Y (13 at.%). According to EDS analysis and estimation of average atomic weight, phase I, II and III have been assigned to Fe_3Mo_3C and $Cr_{23}C_6$ and bcc-solid solution crystal structure, respectively, in agreement with XRD results shown in Fig. 3. XRD patterns of as-cast ingot are shown in Fig. 3. An increase in the volume fraction of M_6C phase was observed in the top of as-cast ingot, where the liquid experienced a slow, but it progressively disappear for higher quenching rates. Microstructures of $Fe_{48}Cr_{15}Mo_{14}Y_2C_{15}B_6$ as-cast samples taken from the top and the middle parts of the ingot are shown in Fig. 2(e and f), respectively. Even in this case the microstructure is refined as the diameter decreased, because of the increased quenching rate. Phase III disapeared in as-cast samples. In Fig. 2(e), EDS analysis showed again that only the phase I contains Y (9 at.%) suggesting a dissolution of Y in the M_6C phase. From Fig. 2(f), SEM/EDS analysis showed similar results for the middle part of as-cast ingot, a part from a reduced crystal sizes because of the increased quenching rate. M_6C phase became rare and decreased in size. The bottom part of the ingot shows a partially amorphous structure, as evidenced from the XRD pattern shown in Fig. 3. Even in this case, crystal phases could not be observed by SEM on bottom part of as-cast sample. Because this part of the sample has a partially amorphous structure, it is possible that the phase compositions are too close to each other so that the contrast relative to the phases could not be achieved.

Fig. 4 shows the XRD patterns for samples with the same composition as Fig. 3, but in this case the casting was performed in cleaner conditions, with a residual vacuum of 10^0 Pa. The master alloy shows the same phase mixture as in Fig. 3. Only a broad halo without any evidence of crystalline peaks was observed, in the bottom part of the as-cast sample, indicating that it consists of a fully amorphous structure. However, with the increase of diameter of the ingot, some sharp crystalline peaks corresponding to $M_{23}C_6$ phases are superimposed to the main halo, implying that the samples has a partially amorphous structure. This result suggests that $M_{23}C_6$ is the last crystal phase nucleating from a deeply undercooled liquid.

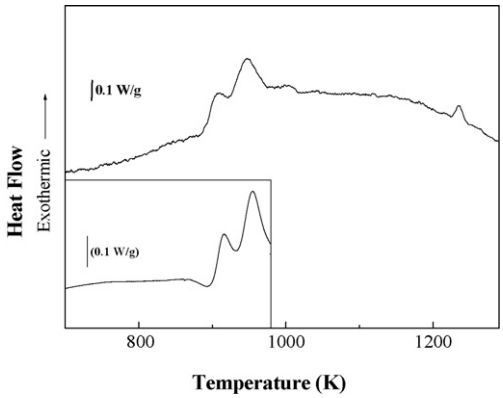

Fig. 5. DSC crystallisation traces for $Fe_{48}Cr_{15}Mo_{14}Y_2C_{15}B_6$ amorphous alloy determined at a heating rate of 0.17 K/s.

Table 1
Results from thermal analysis of $Fe_{50}Cr_{15}Mo_{14}C_{15}B_6$ and $Fe_{48}Cr_{15}Mo_{14}Y_2C_{15}B_6$ alloys

Alloys	T_g (K)	T_x (K)	T_m (K)	T_l (K)	ΔH_x (kJ mol^{-1})	ΔH_m (kJ mol^{-1})
$Fe_{50}Cr_{15}Mo_{14}C_{15}B_6$	–	–	1384	1506		12.7
$Fe_{48}Cr_{15}Mo_{14}Y_2C_{15}B_6$	881	904	1384	1470	7.9	12.3

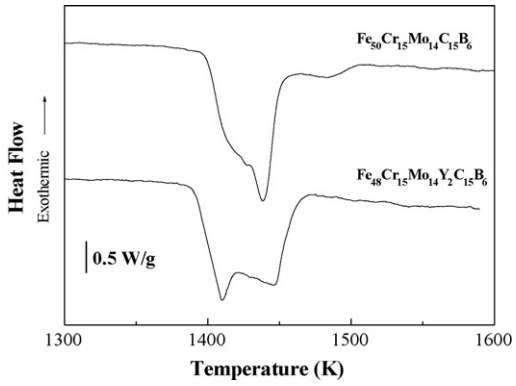

Fig. 6. HTDSC traces for melting of $Fe_{50}Cr_{15}Mo_{14}C_{15}B_6$ and $Fe_{48}Cr_{15}Mo_{14}Y_2C_{15}B_6$ as-cast samples determined at a heating rate of 0.17 K/s.

According to XRD patterns and SEM results, the beneficial effects of addition of Y on glass formation have been evidenced. A higher residual vacuum in the chamber during sample preparation also promotes glass formation.

The crystallisation behavior of the $Fe_{48}Cr_{15}Mo_{14}Y_2C_{15}B_6$ amorphous sample has been studied by DSC at a heating rate of 0.17 K/s and the results are shown in Fig. 5. Table 1 summarized the results obtained from thermal analysis. In order to analyse the crystallisation, the DSC run has been performed by high temperature DSC, as shown in Fig. 5. In order to identify glass transition (T_g) temperature, the experiment was repeated with the same scanning rate for the same as-cast sample by a low temperature DSC, as shown in the inset of Fig. 5. The glass transition temperature was observed at 881 K. The crystallisation gives various overlapped exothermic peaks. The crystallisation products likely constitute a metastable mixture, as evidenced by the small exothermic peak at about 1200 K [5].

In order to understand the effect of Y addition on glass formation, melting behaviors of the alloys have been studied by HTDSC at a heating rate of 0.17 K/s and the results are shown in Fig. 6. The onset melting temperature (T_m) and offset melting temperature T_l (apparent liquidus temperature) for these two alloys are listed in Table 1. Both alloys exhibit non-eutectic melting. In order to identify endothermic effects observed in DSC runs, a pseudo-binary phase diagram was calculated by THERMO-CALC software. Because of the absence of thermodynamic information in the database for high B content, the nominal at.% of metals (Fe, Mo and Cr) were used in the calculation and the phase diagram was plot as a function of C%. During melting, three major endothermic peaks are observed for alloy without the addition of yttrium. $M_{23}C_6$ phase transformed to fcc at around 1283 K. So the first peak at an onset temperature of 1384 K is due to the melting of an fcc phase. The second peak is ascribed to the melting of M_6C phase and third peak is due to the final melting of M_7C_3 phase. The melting behavior of the alloy with yttrium addition showed the same melting temperature, but the suppression of the third peak and a decreasing in the offset melting point (liquidus temperature) (see Table 1). Even in this case, the first peak at an onset temperature of 1384 K is due to the melting of an fcc phase. Because of the absence of a liquidus point, the second peak is ascribed to the eutectic melting of M_6C and M_7C_3 phases. Such eutectic melting, with consequent decrease in the liquidus temperature may be responsible for the enhancement of GFA in the Y containing alloy [6].

4. Conclusions

Glass formation and thermal stability have been studied in $Fe_{50}Cr_{15}Mo_{14}C_{15}B_6$ and $Fe_{48}Cr_{15}Mo_{14}Y_2C_{15}B_6$ alloys. Sample preparation conditions play an important role for the amorphisation. The bottom part of the as-cast sample has a fully amorphous structure when casting was performed with a residual vacuum of 10^0 Pa, whereas it was partially amorphous when casting was performed with a residual vacuum of 10^3 Pa. A high residual vacuum during sample preparation promotes glass formation. The effect of quenching rate on bulk glass formation in alloys has been related to sample dimensions. XRD patterns of the samples with increasing diameter showed decreasing amorphous fraction. The addition of Y leads to a melting behavior of as-cast samples close to eutectic. The addition of 2% Y in $Fe_{50-x}Cr_{15}Mo_{14}Y_xC_{15}B_6$ alloy can improve GFA via lowering liquidus temperature.

Acknowledgements

This work was performed for COFIN/MIUR 2002030504_004 and for MCRTN-CT-2003-504692.

References

[1] A. Inoue, Bulk Amorphous Alloy, Preparation and Fundamental Characteristics, Trans Tech Publications Ltd., Zurich, 1998.
[2] Z.P. Lu, C.T. Liu, J. Mater. Sci. 39 (2004) 3965.
[3] Z.P. Lu, C.T. Liu, J. Mater. Res. 19 (2004) 92.
[4] V. Ponnambalam, S.J. Poon, J. Mater. Res. 19 (2004) 3046.
[5] V. Ponnambalam, S.J. Poon, J. Mater. Res. 19 (2004) 1320.
[6] Z.P. Lui, C.T. Liu, J.R. Thompson, W.D. Porter, Phys. Rev. Lett. 92 (2004) 245503.